Hindawi
Journal of Food Biochemistry
Volume 2024, Article ID 7652471, 12 pages
https://doi.org/10.1155/2024/7652471

Research Article

Network Pharmacology Prediction and Metabolomics Validation of the Novel Targets of *Morus alba* L. against High-Fat Diet-Induced Diabetes Mellitus in C57/6J Mice

Fan Qiu,[1] **Yu-Ping Chen**,[2] **Hong-Yan Wu**,[3] **and Ji-Hu Sun**[3]

[1]*Department of Chinese Medicine, Jiangsu Vocational College of Medicine, Yancheng, China*
[2]*Department of Basic Medical Science, Jiangsu Vocational College of Medicine, Yancheng, China*
[3]*Institute of Medical Biotechnology, Jiangsu Vocational College of Medicine, Yancheng, China*

Correspondence should be addressed to Ji-Hu Sun; ywjkjc1@163.com

Received 25 January 2023; Revised 31 December 2023; Accepted 8 April 2024; Published 2 May 2024

Academic Editor: Mohamed Afifi

Diabetes mellitus (DM) is an endocrine-metabolic disorder that has limited approaches to treat effectively. *Morus alba* L., also known as mulberry, is a well-known medicinal plant, and its branch bark has shown hypoglycemic activity. It is rich in antioxidant and anti-inflammatory ingredients. In this study, we used metabolomics combined with network pharmacology to investigate the molecular mechanism and potential key targets of mulberry branch bark powder (MBBP) for treating DM. Serum metabolomics was performed to analyze the differences in metabolites and enrich metabolic pathways. Network pharmacology, based on systems biology tools, was applied to generate the pathway-target-compound network. Integrated analyses were then used to screen for key targets. To verify the obtained key targets, we used a molecular docking method and experimental validation. Our findings revealed that thirty-five endogenous metabolites contributed to the therapeutic impact of MBBP against DM. The analysis of 10 hub genes in the compound-target network partially supported the enrichment of metabolic pathways. Further analysis focused on two compounds (eugenol and mulberrofuran A) and three key targets (NOS2, MAOA, and CYP1A1). This study explores the active compounds of MBBP against DM and provides a novel perspective for improving DM treatment based on key targets.

1. Introduction

Due to its chronic debilitating character, type 2 diabetes mellitus (T2DM) is known to be diverse [1]. Although twelve drug classes regulate blood glucose approved by the US Food and Drug Administration (FDA), drug side effects continue to be concerning [2]. As a common chronic ailment worldwide, it puts a heavy financial and medical burden on healthcare [3].

Chinese herbal *Morus alba* L. is gaining more attention due to its beneficial medical effects in treating diabetes mellitus (DM) [4, 5]. Its extracts and active components have many positive biological effects such as inhibition of alpha-glucosidase, antioxidant effect, neuroprotective activity, and anticancer properties [6–8]. In our previous research, mulberry branch bark powder (MBBP) demonstrated effective hypoglycemic action [9, 10], but the mechanisms and targets have not been fully elucidated.

MBBP is mainly composed of phenols, flavonoids, coumarins, alkaloids, and polysaccharides [11], and its mode of action has not been explored by network pharmacology-based strategies. In this study, chemical compounds in MBBP were identified and their matching targets were collected and predicted, and then, the signaling pathways were enriched and their impact on the DM network was assessed (Figure 1). A metabolomics method based on UPLC-QTOF/MS combined with multivariate data analysis was established to identify differential metabolites related to the hypoglycemic effect of MBBP on diabetic mice, and then, the relevant metabolic pathway analysis was performed to investigate the hypoglycemic mechanism of MBBP. The metabolomic enzymes in disturbed metabolic pathways were

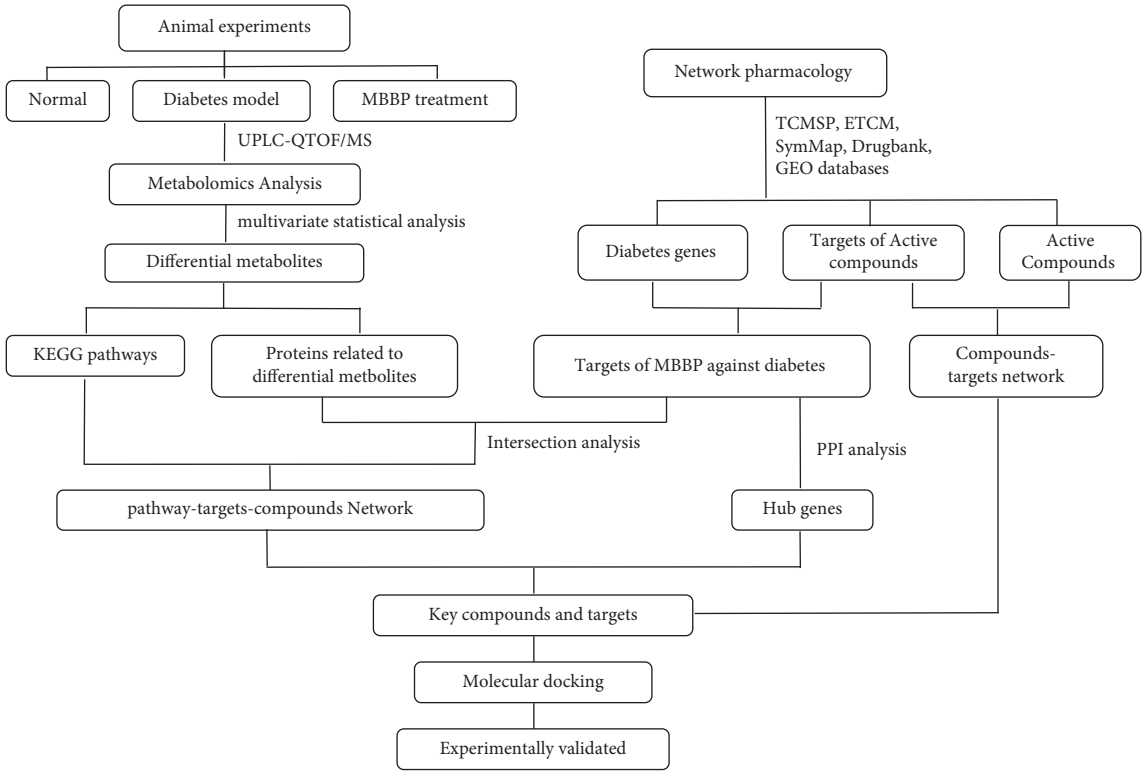

Figure 1: The schematic flowchart of the integrated strategy.

combined with the drug targets in the compound-target network to analyze the potential therapeutic targets [12]. To our knowledge, this was the first to use network pharmacology and metabolomics to explore the targets of MBBP in DM therapy. This study offers fresh insight into the hypoglycemic effects and targets of MBBP in the treatment of DM.

2. Materials and Methods

2.1. Reagents and Materials. Streptozotocin (STZ, S0130) was obtained from Sigma-Aldrich Fine Chemicals, USA. Ammonium acetate, ammonium hydroxide, acetonitrile, and methanol were obtained from CNW Technologies GmbH (Düsseldorf, Germany). 2-Chloro-L-phenylalanine was obtained from Shanghai Hengbai Biotechnology Co., Ltd. (Shanghai, China; purity: ≥98%). All other chemicals and solvents were of analytical or HPLC grade.

Morus alba L. branches were gathered from the mulberry garden in Suzhou, China, in 2019. The bark from the mulberry branches was scraped, dried, and crushed into powder. The powder was weighed and blended with a regular diet to get a 10% MBBP diet for mice, which was optimized according to previous research [9].

Dulbecco's modified Eagle's medium (DMEM), penicillin and streptomycin, phosphate-buffered saline (PBS), and lysis buffer for WB were purchased from Yeasen (Shanghai, China). Fetal bovine serum (FBS), 5-hydroxytryptamine (5-HT), lipopolysaccharide (LPS), and dimethyl sulfoxide (DMSO) were purchased from Sigma-Aldrich (St. Louis, USA). Mulberrofuran A and eugenol were purchased from Naturewill Biotechnology Co., Ltd. (Sichuan, China). The ELISA kits for NOS2 and MAOA were purchased from PYRAM (Shanghai, China). For positive control, the MAOA inhibitor (phenelzine) and the NOS2 inhibitor (L-canavanine sulfate) were purchased from Macklin Biochemical Technology Co., Ltd. (Shanghai, China). The antibodies for NOS2 and MAOA were purchased from Abcam (Cambridge, MA, USA). The antibody for β-actin was purchased from Bioss, China.

2.2. Animals and the Controlled DM Model. Six-week-old male C57/6J mice were obtained from Jiangsu KeyGEN BioTECH Corp., Ltd. (Nanjing, China). All mice were kept in an air-conditioned room at 25°C, and they had free access to food and drink. All procedures were approved by the Institutional Animal Care and Use Committee (Protocol Code: SYXK 2018-0008). Mice were randomly assigned to 3 groups: the normal control group (normal), the high-fat diet and STZ injection group (model), and the 10% MBBP-treated group (treated). The dose of 10% MBBP is the effective dose determined in the previous study [9]. The mice in the normal group were fed a normal laboratory diet. The mice in the model group and the treated group were fed a high-fat diet for five weeks before being given an intraperitoneal injection of STZ (80 mg/kg) in citrate buffer solution (pH = 4.5) [10]. Then, the mice in the model group and the treated group were given a high-fat diet and a 10% MBBP diet for another five weeks, respectively.

Fasting blood glucose (FBG) was assessed using tail-vein sampling by a glucose meter from Johnson & Johnson Medical (Shanghai) Ltd. In the end, the mice were anesthetized with diethyl ether, and blood was taken by eyeball extirpating. Blood samples were kept at 4°C overnight, centrifuged at 3000 rpm for 15 min at 4°C, and then stored at −80°C for further use. Biochemical indices such as the total cholesterol and triglyceride in serum were measured using a BS-800 Chemistry Analyzer (Mindray Medical International Ltd., Shenzhen, China).

2.3. LC-MS Metabolomics Analysis

2.3.1. Sample Preparation. After thawing at room temperature, 20 μL serum sample was added to the EP tube with 200 μL methanol, which was kept at −20°C before extraction, and treated with ultrasound for 10 min in ice water. Following incubation at −20°C to precipitate proteins, the samples were centrifuged at 12000 rpm for 15 min, and the fresh supernatant was transferred into EP tubes. About 10 μL aliquots from each sample were combined to create the QC sample. The extracts are dried in a vacuum concentrator. Then, 1000 μL of reconstitution liquid was added for the extraction (V acetonitrile: V water = 1 : 1), vortexed for 30 s, and sonicated for 10 min in a water bath at 4°C. After 15 minutes of centrifugation at 13000 rpm at 4°C, 60 μL of the supernatant was transferred into a 2 mL LC/MS glass vial for the UHPLC-QTOF/MS analysis, and the QC sample was inserted into every five samples to check the stability of the instrument [13, 14].

2.3.2. UPLC-QTOF/MS Analysis. The analyses were carried out using a TripleTOF 6600 (QTOF, AB Sciex) connected to a UPLC system (1290, Agilent Technologies) with a BEH Amide Column (1.7 μm 2.1∗100 mm, Waters). The mobile phase contained 25 mM NH_4OAc and 25 mM NH_4OH in water (pH = 9.75) (A) and acetonitrile (B) and was conducted with a linear gradient as follows: 0 min, 95% B; 15 min, 65% B; 25 min, 40% B; 25.1 min, 95% B; and 30 min, 95% B. The flow rate was 0.5 mL min^{-1}. In information-dependent acquisition (IDA) mode, one cycle encompassed a full-range MS scan (80–800 m/z) followed by 12 MS/MS scans whose intensity was greater than 100. ESI source gas 1 and gas 2 were set as 60 Psi; curtain gas was set as 35 Psi; source temperature was set as 650°C; and ion spray voltage floating (ISVF) was set as 5000 V/−4000 V in positive or negative modes, respectively.

2.3.3. Data Analysis. ProteoWizard was used to convert MS raw data files to mzXML format, and R package XCMS was used to produce a data matrix that was composed of the retention time (RT), mass-to-charge ratio (m/z) values, and peak intensity. Peak annotation was performed using R package CAMERA. Peak intensities were normalized and imported into SIMCA 14 (Umetrics, Sweden). The PCA was performed after unit variance scaling. The OPLS-DA was performed after pareto scaling. The threshold of VIP values (VIP >1) and t-test ($P < 0.05$) was used to determine the differential metabolites between the model group and the normal group, the treated group, and the model group.

2.4. Network Pharmacology Construction

2.4.1. Mulberry Bark Compounds and Their Putative Targets. The information on compounds was mainly obtained from TCMSP, ETCM databases, and related literature. The oral bioavailability (OB) (≥30%) and drug-likeness (DL) (≥0.18) of active compounds were marked (Table S3). Putative targets of each compound were predicted from databases: (1) DrugBank (https://www.drugbank.ca), (2) TCMSP (Traditional Chinese Medicine Systems Pharmacology Database) (https://lsp.nwu.edu.cn/tcmsp.php), (3) SymMap (Symptom Mapping) (https://www.symmap.org/), and (4) ETCM (Encyclopedia of Traditional Chinese Medicine) (https://www.nrc.ac.cn:9090/ETCM/).

2.4.2. DM-Associated Genes and Drug Target Proteins. Searching the DrugBank database with the disease name "Diabetes Mellitus" (id C0011849), 1506 DM-associated genes were obtained. A genomic expression profile for DM in the GEO database (dataset GSE38642) was analyzed, and 109 differentially expressed genes were identified (P value < 0.05, logFC >0.585, and logFC < −0.585). Additionally, 8 DM-related drugs and their 42 target proteins were also collected from the DrugBank database.

2.4.3. Network Construction. Cytoscape 3.7.2 was used to construct the network (Cytoscape Construction, CA, USA). Two visualized networks were built: (1) compound-target network, which consisted of active compounds in MBBP and their targets, and (2) KEGG pathway-target-compound network, which is based on differential metabolite analysis.

2.5. Molecular Docking. The crystal structures of targets were downloaded from the RCSB Protein Data Bank (https://www.rcsb.org/): NOS2, PDB ID: 3E7G; MAOA, PDB ID: 2Z5Y; and CYP1A1, PDB ID: 4I8V. The ligands' structures of eugenol and mulberrofuran A were obtained from the PubChem database. After removing water molecules and adding hydrogen atoms, the structure files were converted into pdbqt formats with AutoDockTools 1.5.6. The docking calculations used the genetic algorithm. Molecular mechanics force fields were also used to find low-energy conformation. The most suitable docking orientation with the lowest energy level was visualized by PyMOL.

2.6. Experimental Validation

2.6.1. ELISA. The activity of NOS2 and MAOA in mouse plasma was measured using enzyme-linked immunosorbent assay (ELISA) kits obtained from PYRAM (PM103770-96T and PM105552-96T) according to the manufacturer's instructions.

2.6.2. Cell Culture and Cell Viability. The HepG2 (human hepatocarcinoma) cell line was recovered from freezing and cultured in DMEM supplemented with 10% FBS and 1% penicillin/streptomycin at 37°C in a 5% CO_2 atmosphere. When cells reached 5×10^4 cells/mL after several passages, they were divided into the control group (cells treated with DMEM), the NOS2-positive group (cells treated with 10 μg/mL LPS for 24 h), the MAOA-positive group (cells treated with 10 μg/mL 5-HT for 48 h), and the drug treatment groups (10 μg/mL LPS + mulberrofuran A, 10 μg/mL LPS + eugenol, and 10 μg/mL 5-HT + eugenol). Cell viability was determined using a CellTiter-Lumi Plus Kit (Beyotime, China) according to the manufacturer's instructions.

2.6.3. Western Blot Analysis. Cells were collected and split on ice with RIPA buffer containing protease inhibitors for 30 minutes, and the cellular lysate was then centrifuged at 12,000 rpm for 15 min at 4°C. The supernatants were collected, and loading buffer was added to the supernatant and boiled in a 95°C metal bath for 15 minutes to denature the protein sample. The protein concentrations were determined by the BCA Protein Assay Kit (P0010, Beyotime, China). The same amount of protein sample was separated by SDS-PAGE gel and transferred to the PVDF membrane. After sealing, it was incubated with the first antibodies against MAOA (1 : 1000 dilution, ab126751), NOS2 (1 : 1000 dilution, ab178945), and β-actin (1 : 5000 dilution, bs-0061R) in a refrigerator at 4°C overnight. After washing the membrane, incubating the secondary antibody, and washing the membrane again, it was visualized using ECL (Millcore).

3. Results

3.1. MBBP Treatment Improves Many Biochemical Indexes in DM Mice. As shown in Figure 2(a), the model group's fast blood glucose level was higher than that of the normal group. The 10% MBBP-treated group showed reduced fast blood glucose levels, and the average blood glucose level in the treated group was close to that in the normal group. The result indicated that MBBP had a role in lowering plasma glucose concentrations.

Seventeen biochemical parameters were measured on each mouse (Table S1), and PCA was performed to find trends among them (Figure 2(b)). The PCA model has two components with $R^2X(\text{cum}) = 0.455$, indicating a stable model. Q2 is 0.0397, which means the pattern's predictive ability is low. In the score plot, the normal group and model group were completely separated and the normal group was near the MBBP-treated group. This indicates that the sick state in the model group could be improved by MBBP feeding in mice. By analyzing the loading plot (Figure 2(c)), the lipid metabolism indexes of CHOL (total cholesterol), HDL-C (high-density lipoprotein cholesterol), and LDL-C (low-density lipoprotein cholesterol) are up on the oblique axis of the second quadrant, which means they are increased in the model group when compared to those of the normal and treated groups. CHOL correlates positively with HDL-C and negatively with INS (insulin) levels. The loading plot also shows that UA (uric acid) and CHE (cholinesterase) have a high positive correlation, while TG (triglyceride) and ALT (alanine aminotransferase) correlated negatively with GGT (glutamyl transferase).

3.2. Metabolomics Profiling. There are a lot of LC-MS data, and multivariate analysis was carried out to find trends and potential biomarkers. In the PCA score plot, the overlap of the quality control (QC) indicated steady instrument behavior throughout the run (Figure 3(a)). The normal group and the model group were divided, and the MBBP-treated group was relatively similar to the normal group. This demonstrated metabolic disruption brought on by a high-fat diet, and STZ was reversed following MBBP feeding in mice. In the OPLS-DA (orthogonal partial least-squares discriminant analysis) score plot, the treated group and the model group were kept apart (R2Y (cum) = 0.999 and Q2 (cum) = 0.889), as shown in Figure 3(b). The S-plot of OPLS-DA revealed a range of metabolites, and the differential metabolites are listed in Figure 3(d), which were determined by variable importance in the projection (VIP) value (VIP >1) and the corresponding P values ($P < 0.05$). There are 35 differing metabolites in the model group that were chosen in comparison with the MBBP-treated group (Table S2). To investigate impacted metabolic pathways, enrichment analysis was carried out by importing these differential metabolites into MetaboAnalyst 5.0 (https://www.metaboanalyst.ca/). The significant perturbed metabolic pathways are listed in Figure 3(e), including aspartate metabolism, cysteine metabolism, urea cycle, glucose-alanine cycle, alanine metabolism, and glutamate metabolism.

3.3. The Bioactive Compound-Target Network Analysis. There are 43 bioactive chemicals from MBBP listed in Table S3, and only 7 compounds met the drug screening criteria of oral bioavailability (OB) ≥ 30% and drug-likeness (DL) ≥ 0.18. There are 257 targets corresponding to the bioactive compounds collected from the DrugBank, TCMSP, SymMap, and ETCM databases. The compound-target network was refined according to the degree value of nodes that were generated after the topological analysis (Figure 4(e)). The important compound nodes in the network include kaempferol (degree = 34), resveratrol (degree = 28), eugenol (degree = 18), cyclomulberrochromene (degree = 10), morin (degree = 9), mulberrofuran A (degree = 8), cularicine (degree = 8), sesamol (degree = 6), and 3,4,5-trimethoxytoluene (degree = 6).

3.4. Identification of MBBP's Important Targets by Intersection Analysis. We investigated the overlaps between disease genes from the DrugBank database, differentially expressed genes in the GSE38642 dataset, drug targets from the DrugBank, and compounds' targets mainly from the TCMSP and ETCM databases. As shown in Figure 4(a), 26 disease genes in the disease gene set were differentially expressed in T2DM patients, and among them, 4 genes are

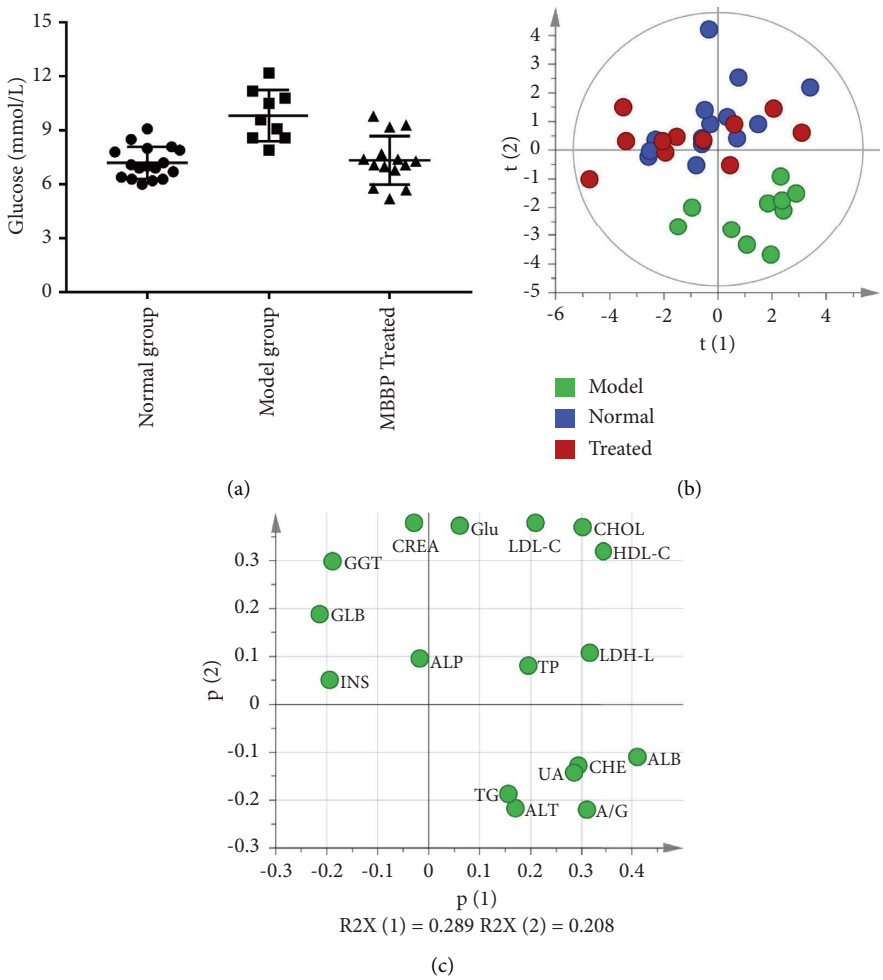

Figure 2: The common serum biochemical indicators in mice. (a) The serum level of fast glucose; (b) principal component analysis (PCA) score plots; (c) loading scatter plot (Glu, glucose; CREA, creatinine; GGT, γ-glutamyl transpeptidase; GLB, globulin; INS, insulin; ALP, alkaline phosphatase; TG, triglyceride; ALT, alanine aminotransferase; UA, uric acid; CHE, cholinesterase; ALB, albumin; A/G, globulin ratio; TP, total protein; HDL-C, high-density lipoprotein cholesterol; LDL-C, low-density lipoprotein cholesterol; LDH, lactic dehydrogenase; CHOL, cholesterol).

MBBP compounds' targets. There are 7 drug targets in MBBP compounds' targets. In the following study, we use the 106 targets in both the compound-target set and the disease gene set.

DAVID was used to conduct functional annotation and pathway enrichment for the 106 genes (Figure 4(d)). GO analysis showed that the targets were mainly enriched in biological process (BP): response to oxidative stress, reactive oxygen species, and nutrient levels; molecular function (MF): nuclear receptor activity, heme binding, and NADP binding; and cellular component (CC): membrane region, membrane microdomain, and membrane raft. KEGG pathway analysis showed that these targets were mainly enriched in IL-17 signaling pathway, fluid shear stress and atherosclerosis, and AGE-RAGE signaling pathway in diabetic complications.

The interactions of the 106 targets were analyzed using STRING tools. The PPI network includes 106 nodes and 1370 edges (Figure S1), and the top ten hub genes ranked by Maximal Clique Centrality (MCC) and EcCentricity in the cytoHubba plugin were identified (Figures 4(b) and 4(c)).

3.5. Integrated Analysis of Metabolomics and Network Pharmacology. To further improve the accuracy of the active compound screening, the metabolic pathways indicated by differential metabolites are considered references. OmicsNet (https://www.omicsnet.ca/) was used to collect the metabolism-related genes. By matching the compounds' targets with the genes associated with metabolites, it was found that there were several key targets, including NOS2, MAOA, CYP1A1, GOT2, COMT, and PLA2G2A (Table S4). The main metabolites involved oxoglutaric acid, L-cysteine, citrulline, norepinephrine, and linoleic acid. NOS2 is the hub gene, and MAOA is in the overlap of drug targets, disease genes, and compound targets. These results showed that MBBP regulated metabolic pathways with different active compounds; among them, central carbon metabolism,

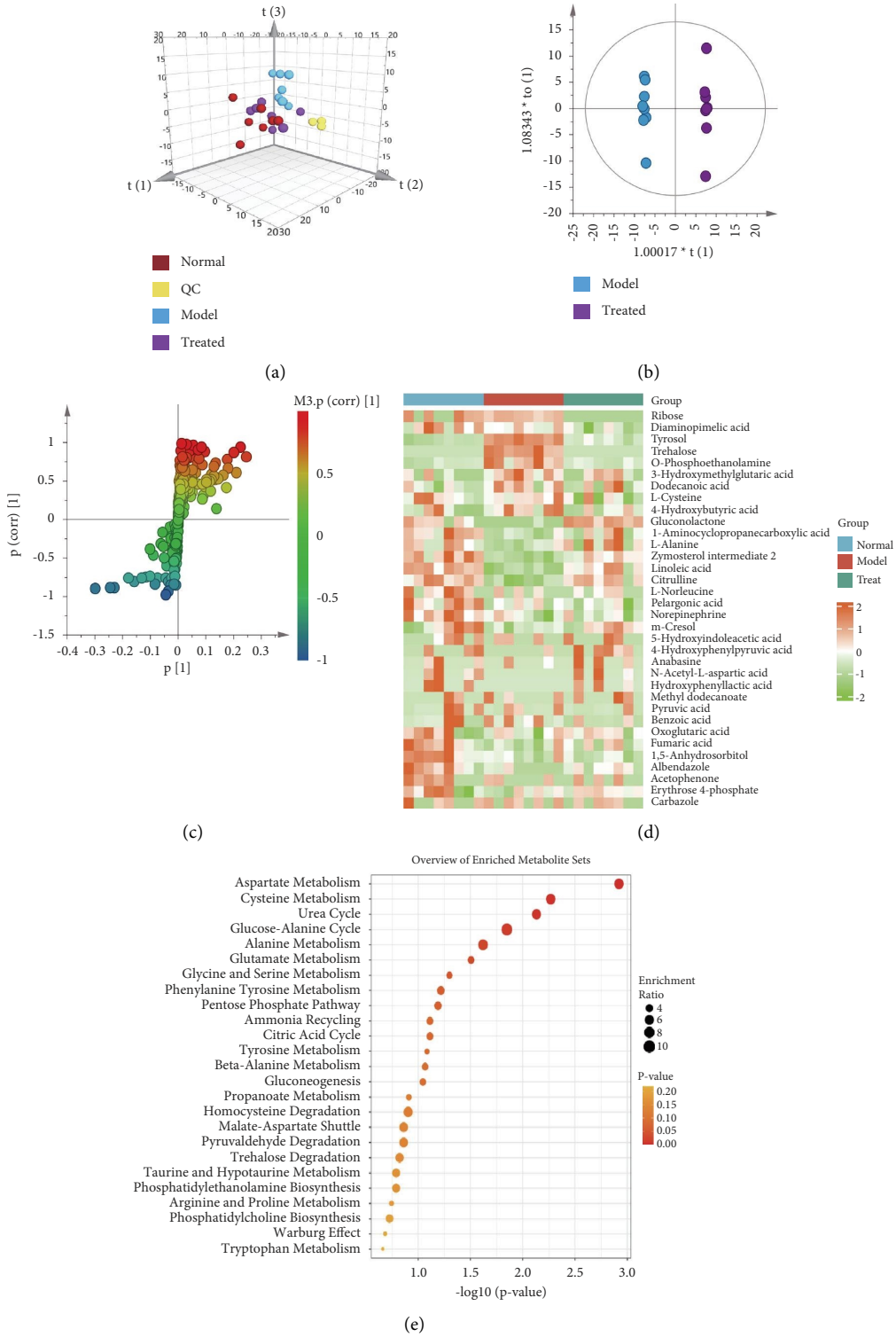

Figure 3: Multivariate statistical analysis of metabolomics data. (a) The PCA score plot of all groups; (b) OPLS-DA score plots; (c) S-plot for discriminating the metabolite; (d) heatmap showing the differentially expressed primary metabolites; (e) the enrichment analysis of metabolite. Node size is based on enrichment ratio, and node color is based on *P* value.

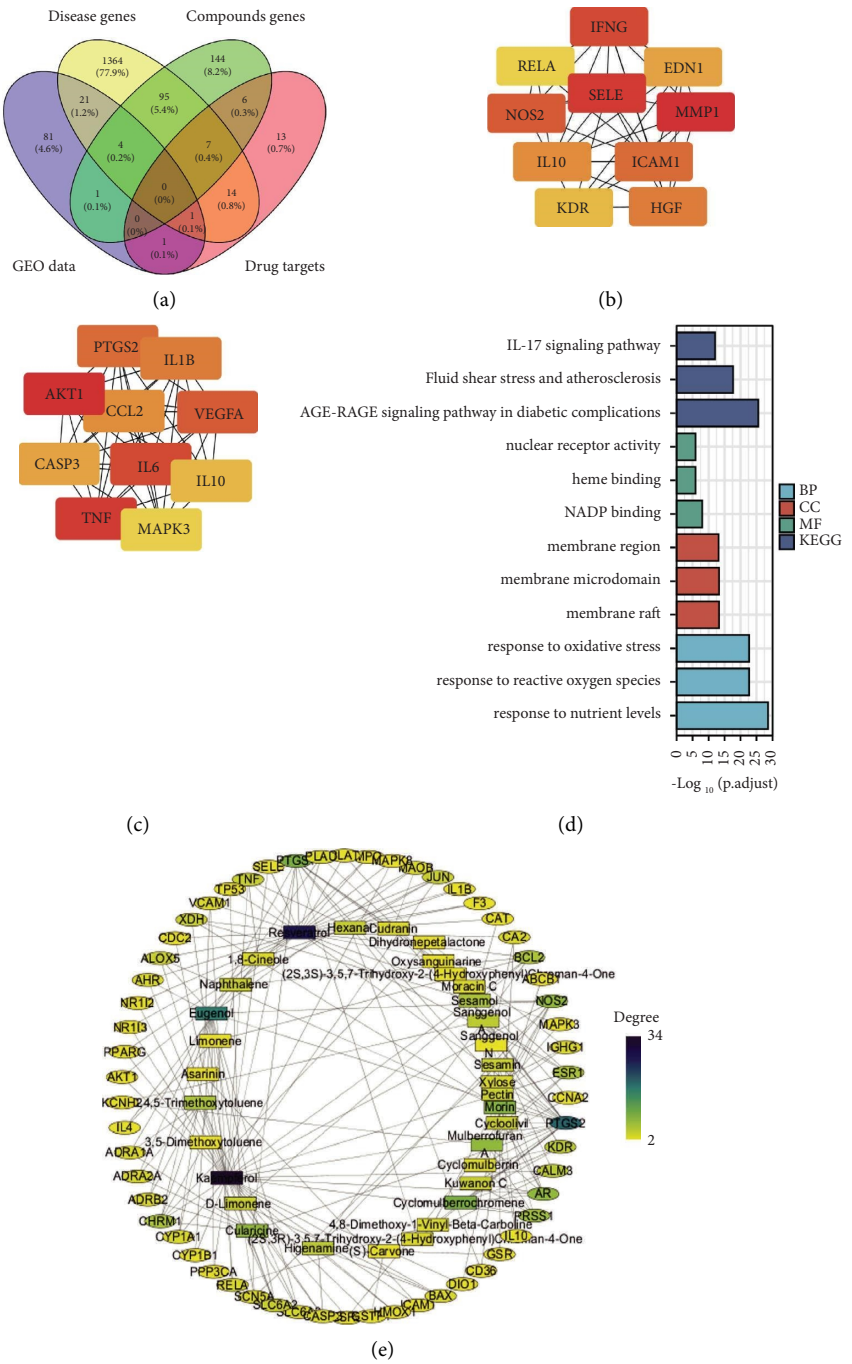

Figure 4: (a) Overlap between disease genes from the DrugBank database (disease gene), differentially expressed genes from the GSE38642 dataset (GEO data), drug targets from the DrugBank (drug targets), and compounds' targets mainly from the TCMSP and ETCM databases (compound targets); (b) top ten hub genes in 106 genes ranked by Maximal Clique Centrality (MCC) in cytoHubba plugin of Cytoscape; (c) top ten hub genes in 106 genes ranked by EcCentricity in cytoHubba plugin of Cytoscape; (d) significantly enriched GO terms and KEGG pathways of 106 genes from overlaps of compound targets and disease genes (BP, biological process; CC, cellular component; MF, molecular function; KEGG, Kyoto Encyclopedia of Genes and Genomes); (e) compound-target network. The square nodes represent the bioactive compounds, the oval nodes represent the predicted targets, and the color of the nodes was mapped according to the degree.

protein digestion and absorption, arginine and proline metabolism, tyrosine metabolism, and propanoate metabolism were related to differential metabolites and compounds' targets (Figure 5).

3.6. Molecular Docking. It was noted that eugenol has three targets, NOS2, MAOA, and CYP1A1. Molecular docking was conducted to assess the mode of binding of eugenol with target proteins (Figure 6). The parameters of molecular

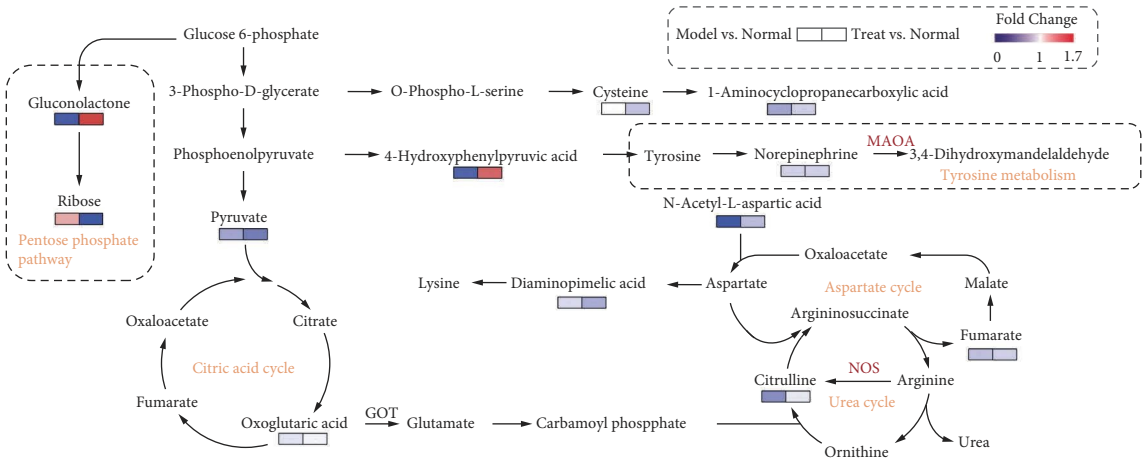

Figure 5: The interaction network based on metabolomics and network pharmacology. Differential metabolites with red color denote an up change, blue denotes a down change when compared with the normal group, and orange denotes a pathway label.

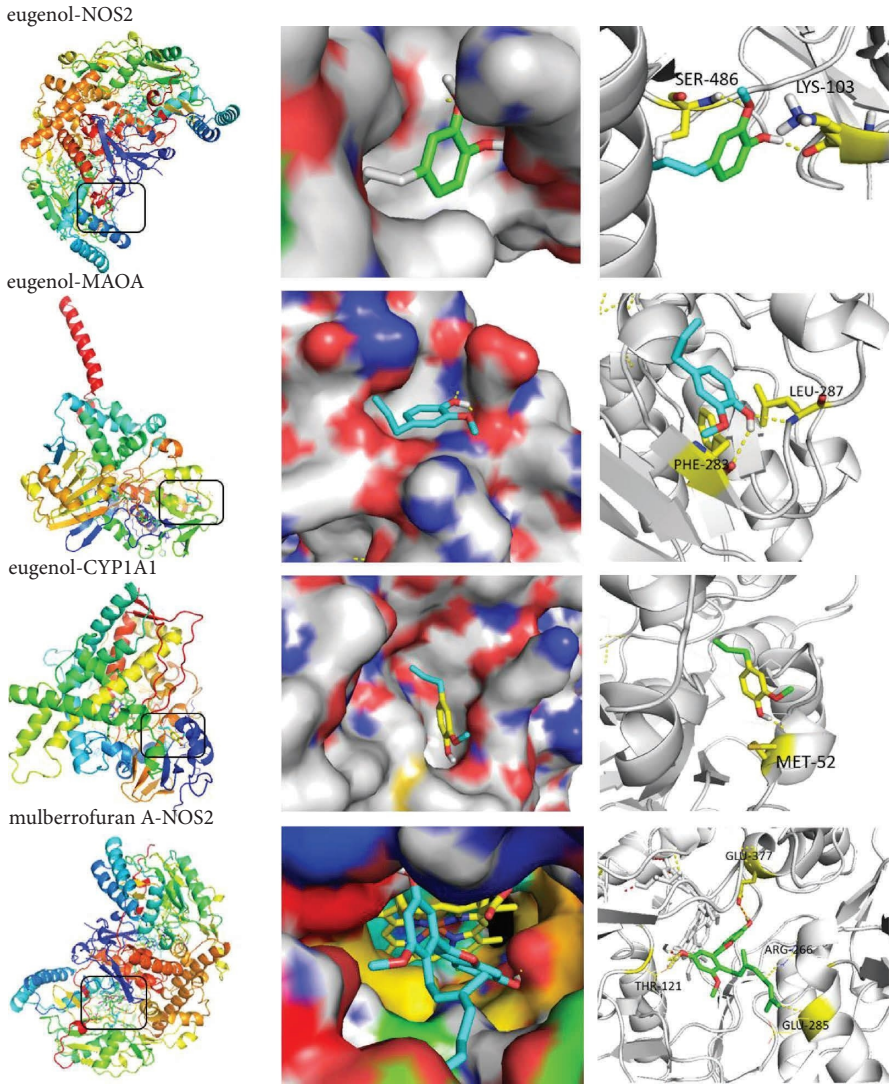

Figure 6: Molecular docking of eugenol and mulberrofuran A with the key targets. List 1, the position of small molecules in the 3D structure of proteins; list 2, the binding location shown as surface structure coloring by element (grey, C H; blue, N; red, O); list 3, the molecular hydrogen-bonding interaction diagram, which was indicated by dotted lines.

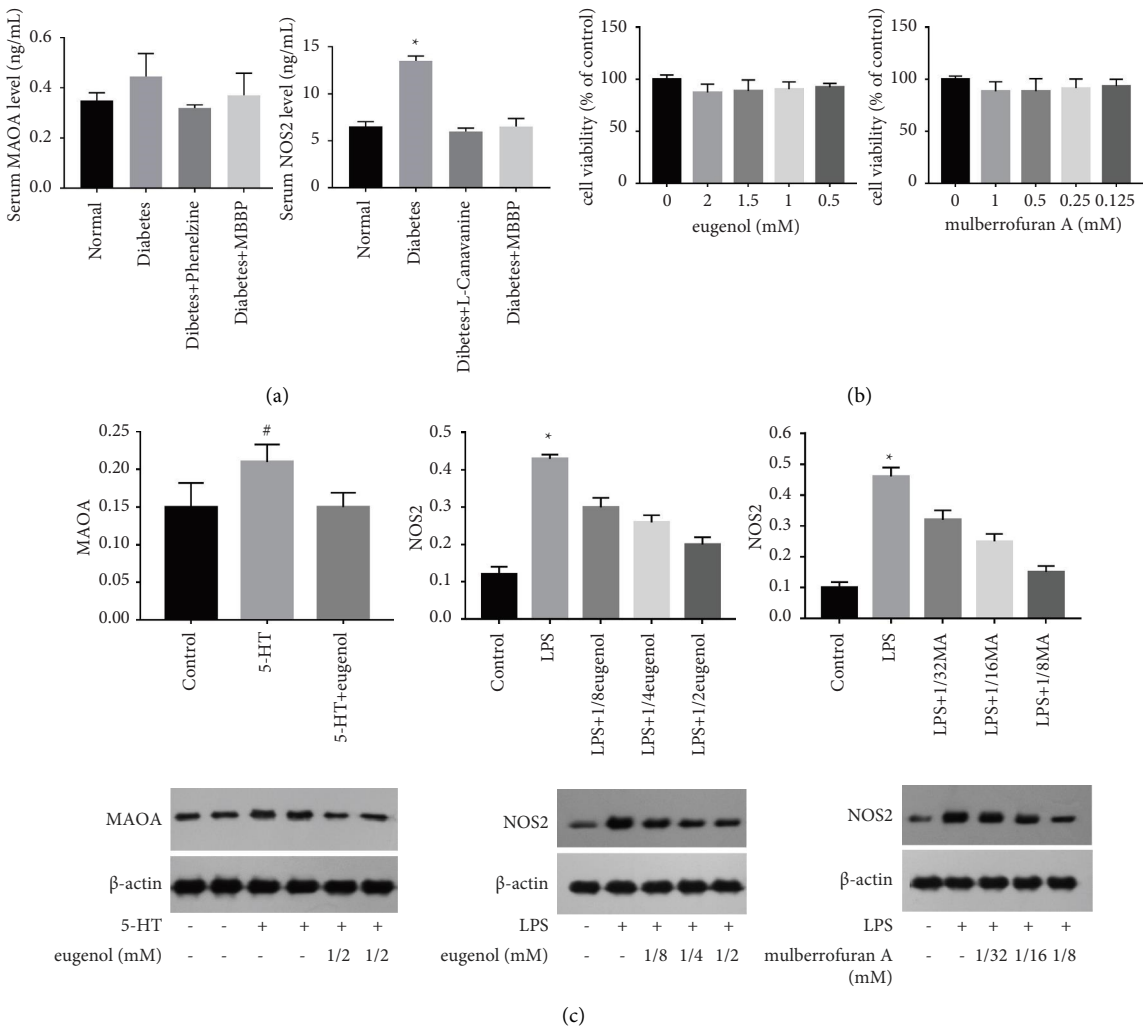

Figure 7: Validation of MAOA and NOS2 targets of eugenol and mulberrofuran A. (a) Expressions of MAOA and NOS2 in mouse plasma using ELISA kits after indicated treatment; (b) cell viability was detected by the CellTiter-Lumi Plus Assay; (c) expression of MAOA and NOS2 proteins in HepG2 cells treated with eugenol and mulberrofuran A for 24 h in the presence of 5-HT or LPS (compared with control group, $^{\#}P < 0.05$, $^{*}P < 0.01$, $n = 4$; MA: mulberrofuran A).

docking between compounds and targets are listed in Table S5. In the interaction with NOS2, eugenol formed hydrogen bonds with LYS-103 and SER-486, which were near the HEM binding site, and the binding energy of eugenol towards NOS2 was −4.44 kcal/mol. In the interaction with MAOA, eugenol formed hydrogen bonds with LEU-287 and PHE-283, which were close to the FAD binding site, and formed a pi-alkyl interaction with HIS282 and ASN292, and the binding energy of eugenol towards MAOA was −3.87 kcal/mol. In the interaction with CYP1A1, eugenol formed hydrogen bonds with MET52, a pi-alkyl interaction with PRO233 and TYR494, which were near the HEM binding site, and a carbon-hydrogen interaction with GLY229 and SER230 in the binding pocket, and the binding energy of eugenol towards CYP1A1 was −4.51 kcal/mol.

We also analyzed mulberrofuran A with NOS2 by molecular docking, and mulberrofuran A made hydrogen-bonding interaction with GLU377 and THR121 and formed carbon-hydrogen interaction with GLU285 and ARG266, which were also near the HEM ring binding site. The binding energy of mulberrofuran A towards NOS2 was −3.83 kcal/mol (Figure 6).

3.7. Targets MAOA and NOS2 Validation. We have investigated the therapeutic effects of MBBP using an animal model of T2DM. Synergetic regulation effects of MBBP were found based on the metabolomics analysis and compound-target network. To further assess the targets of MAOA and NOS2, the level of MAOA and NOS2 in plasma was detected

(Figure 7(a)). Compared with the normal group, the protein expression of MAOA and NOS2 in the DM group was increased. In contrast, treatment with MBBP significantly attenuated the phenomenon in the DM group.

To validate the effect of compounds in MBBP on MAOA and NOS2, we conducted cell-based studies. MAOA and NOS2 are two different enzymes involved in the anabolism of monoamine neurotransmitter and NO, respectively. HepG2 cells capable of expressing these two enzymes were selected. LPS and 5-HT were used as inducers to increase the expression of NOS2 and MAOA, respectively. After 48 h of incubation, the viability effects of mulberrofuran A and eugenol at gradient concentrations were examined on HepG2 cells using the CellTiter-Lumi Plus Assay (Figure 7(b)). The results revealed that eugenol had no significant effect on cell viability at the dose of 0.5 mM (82 μg/mL), and mulberrofuran A had no significant effect on cell viability at the dose of 0.125 mM (50 μg/mL). Western blot analysis has shown that the protein expression of MAOA was significantly suppressed by eugenol when compared to cells in the 5-HT-stimulated alone group. Compared with the LPS group, the protein expression of NOS2 was significantly decreased accompanied by an increased concentration of eugenol and mulberrofuran A, respectively (Figure 7(c)).

4. Discussion

There are a variety of pathophysiological mechanisms that lead to hyperglycemia, which converge on the declined endogenous insulin secretory capacity and the impaired state of glucose metabolism [2, 3]. Inflammation and high oxidative stress are critical facets of DM, which contribute to systemic complications [15]. In this study, the metabonomic data revealed biochemical abnormalities in the model group (Figure 5). The low level of fumarate and oxoglutaric acid in the diabetic-induced model group showed the down-regulated TCA cycle; pyruvate, a product of glycolysis, is decreasing, which reflects abnormal utilization of glucose [16]. In the MBBP-treated group, the high level of gluconolactone and the low level of ribose may indicate the exploitation of the pentose phosphate pathway, which also provides NADPH for counting the damaging effects of oxygen radicals, and the reduced cysteine indicates the increased availability of cysteine to counter oxidative stress [17]. The tyrosine metabolism was also disturbed according to the level of differential metabolites 4-hydroxyphenylpyruvic acid and norepinephrine. The changed level of citrulline in the urea cycle may be related to the generation of NO in arginine metabolism [18]. In general, the changes in metabolites in the model group reflected the impaired metabolism of the pentose phosphate pathway, urea cycle, aspartate cycle, and tyrosine metabolism, and these were alleviated in the MBBP-treated group.

Morus alba L. is a source of bioactive small molecules for its wide range of medicinal properties. The phenolic components such as isoquercitrin, resveratrol, and morin act as antioxidants and tyrosinase inhibitors [19]. 1-Deoxynojirimycin (DNJ) from mulberry trees is an inhibitor of intestinal α-glycosidases [20]. Diels–Alder-type adducts containing prenylated flavonoids showed phosphodiesterase-4 inhibitory activity [21]. Mulberry polysaccharides possess antidiabetic activity and immunomodulatory activity [22]. In this research, the results of combining the analysis of metabolomics and network pharmacology lead us to mainly focus on L-aspartate, mulberrofuran A, eugenol, kaempferol, sesamin, piceid, and naphthalene (Table S4). Considering L-aspartate is an endogenous metabolite, kaempferol widely exists in other plants and has characteristics of targets, and we mainly discuss eugenol, mulberrofuran A, and targets NOS2, MAOA, and CYP1A1 (Figure S2).

The metabolic disorder in DM can lead to a rise in oxygen-free radicals. The oxidative stress caused by excessive oxygen-free radicals can cause toxicity to the vascular endothelium [23]. O_2^- reacts with NO to produce $ONOO^-$, which affects the normal function of nitric oxide synthase (NOS), resulting in more NO generation [24]. NOS exists in three subtypes: neuronal-NOS (nNOS/NOS1), endothelial-NOS (eNOS) expressed normally, and inducible-NOS (iNOS/NOS2) induced after injury [25]. NO derived from iNOS/NOS2 and nNOS/NOS1 has neurotoxic effects [26]. Molecular docking shows that eugenol and mulberrofuran A bind tightly with NOS2, indicating that they may reduce oxidative stress-induced inflammatory damage by inhibiting NOS2 and decreasing NO production [27].

Monoamine oxidase (MAO) exists in two isoforms: MAOA and MAOB. MAOB is primarily found in the human brain. MAOA is the predominant form found in the gut and prevents catecholamines in the periphery from activating [28]. MAOA is involved in the breakdown of the neurotransmitters: epinephrine, norepinephrine, and dopamine. MAOA also helps break down monoamines in the diet [29]. It seems to be important in the breakdown of excess tyramine, which is found in cheese and other foods. Lee et al. [30] reported that the expression of the MAOA gene was increased after a high-fat diet. An et al. [31] discovered that regardless of genetic and other clinical factors, methylation variation in the MAOA gene promoter is related to fasting plasma glucose. Solivan-Rivera et al. [32] identified mechanisms that regulate the formation of thermogenic adipose tissue and suggested that human adipocyte MAOA could serve as a potential therapeutic target for metabolic disorders. Our molecular docking analysis of eugenol and MAOA reflected that the hypoglycemic mechanism may be bound up with inhibiting MAOA by eugenol after a high-fat diet.

There are numerous ROS-producing enzymes, such as cytochrome P450 monooxygenases (CYP450s/CYP1A1), whose activities and expressions may be altered under DM circumstances [33]. The hepatic cytochrome CYP1A1 activity was significantly elevated in diabetic rats by a fold of 2.1, according to Gökçe Kuzgun's investigation into the effect of insulin treatment on hepatic cytochrome CYP1A1 [34]. Docked conformation and interactions of the CYP1A1-eugenol complex showed that the regulation of CYP1A1 can be a target for the improvement of DM.

5. Conclusion

In this study, we explore the therapeutic mechanisms of MBBP in treating DM using network pharmacology and metabolomics. Key targets, associated metabolites, and active compounds were all recognized by the integrated study. Molecular docking was used to further validate these targets. Interestingly, there will always be binding sites for these compounds not far from the FAD or HEM in the proteins. According to the changes in metabolites, we paid close attention to the urea cycle, citric acid cycle, aspartate cycle, and tyrosine metabolism and found that NOS2, MAOA, and CYP1A1 were the potential important targets of MBBP to improve DM. There is not much research on DM focusing on MAOA and CYP1A1, and our findings provide a novel perspective to improve the oxidative stress of DM.

Data Availability

The data used to support the findings of this study are available from the corresponding authors upon request.

Conflicts of Interest

The authors declare that they have no known conflicts of interest or personal relationships that could have appeared to influence the work reported in this paper.

Authors' Contributions

Fan Qiu curated the data, involved in formal analysis, designed methodology, provided software, validated the data, visualized the data, wrote the original draft, and reviewed and edited the manuscript. Yu-Ping Chen conceptualized the study, investigated the data, and acquired funding. Hong-Yan Wu conceptualized the study and supervised the data. Ji-Hu Sun conceptualized the study, supervised the data, and acquired funding.

Acknowledgments

This work was financially supported by the China Agriculture Research System fund CARS-22-ZJ0504, the Innovation-Driven Project of Jiangsu Vocational College of Medicine (No. 20200027), and the National Natural Science Foundation of China (No. 81903879). We especially wish to thank Shanghai Biotree Biomedical Technology Co., Ltd., for providing laboratory equipment and technical assistance.

Supplementary Materials

Additional file 1: Figure S1. Protein-protein interaction network constructed with the overlap targets of compound-target and disease gene sets. Figure S2. The subnetwork of the pathway-target-compound network focused on eugenol and mulberrofuran A before gene filtration. Orange, pathway; purple, target; yellow, compound. Additional file 2: Table S1. The common serum biochemical indicators in mice. Table S2. The differential metabolites in MBBP-treated mice. Table S3. The compounds of MBBP. Table S4. The metabolites and related targets and compounds. Table S5. Grid box parameters of molecular docking between eugenol and targets. (*Supplementary Materials*)

References

[1] A. K. Rines, K. Sharabi, C. D. Tavares, and P. Puigserver, "Targeting hepatic glucose metabolism in the treatment of type 2 diabetes," *Nature Reviews Drug Discovery*, vol. 15, no. 11, pp. 786–804, 2016.

[2] W. K. Chung, K. Erion, J. C. Florez et al., "Precision medicine in diabetes: a consensus report from the American diabetes association (ada) and the European association for the study of diabetes (easd)," *Diabetologia*, vol. 63, no. 9, pp. 1671–1693, 2020.

[3] R. Forde, L. Arente, D. Ausili et al., "FEND COVID-19 consortium the impact of the COVID-19 pandemic on people with diabetes and diabetes services: a pan-European survey of diabetes specialist nurses undertaken by the Foundation of European Nurses in Diabetes survey consortium," *Diabetic Medicine*, vol. 38, no. 5, Article ID e14498, 2021.

[4] H. I. Jeong, S. Jang, and K. H. Kim, "*Morus alba* L. for blood sugar management: a systematic review and meta-analysis," *Evidence-based Complementary and Alternative Medicine*, vol. 2022, Article ID 9282154, 10 pages, 2022.

[5] C. Tang, T. Bao, Q. Zhang et al., "Clinical potential and mechanistic insights of mulberry (Morus alba L.) leaves in managing type 2 diabetes mellitus: focusing on gut microbiota, inflammation, and metabolism," *Journal of Ethnopharmacology*, vol. 306, Article ID 116143, 2023.

[6] G. Ma, X. Chai, G. Hou, F. Zhao, and Q. Meng, "Phytochemistry, bioactivities and future prospects of mulberry leaves: a review," *Food Chemistry*, vol. 372, Article ID 131335, 2022.

[7] D. N. H. Tam, N. H. Nam, M. T. Elhady et al., "Effects of mulberry on the central nervous system: a literature review," *Current Neuropharmacology*, vol. 19, no. 2, pp. 193–219, 2020.

[8] E. W. C. Chan, S. K. Wong, J. Tangah, T. Inoue, and H. T. Chan, "Phenolic constituents and anticancer properties of Morus alba (white mulberry) leaves," *Journal of Integrative Medicine*, vol. 18, no. 3, pp. 189–195, 2020.

[9] F. Qiu, J. Wang, H. Y. Liu, and Y. Q. Zhang, "Mulberry bark alleviates effect of STZ inducing diabetic mice through negatively regulating FoxO1," *Evidence-based Complementary and Alternative Medicine*, vol. 2019, Article ID 2182865, 9 pages, 2019.

[10] F. Qiu and Y. Q. Zhang, "Metabolic effects of mulberry branch bark powder on diabetic mice based on GC-MS metabolomics approach," *Nutrition and Metabolism*, vol. 16, no. 1, p. 10, 2019.

[11] S. Wang, M. Fang, Y. L. Ma, and Y. Q. Zhang, "Preparation of the branch bark ethanol extract in mulberry Morus alba, its antioxidation, and antihyperglycemic activity in vivo," *Evidence-based Complementary and Alternative Medicine*, vol. 2014, Article ID 569652, 7 pages, 2014.

[12] T. Li, W. Zhang, E. Hu et al., "Integrated metabolomics and network pharmacology to reveal the mechanisms of hydroxysafflor yellow A against acute traumatic brain injury," *Computational and Structural Biotechnology Journal*, vol. 19, pp. 1002–1013, 2021.

[13] T. Hu, Z. L. An, Y. Sun et al., "Longitudinal pharmacometabonomics for predicting malignant tumor patient responses to anlotinib therapy: phenotype, efficacy, and toxicity," *Frontiers Oncology*, vol. 10, Article ID 548300, 2020.

[14] L. Zuo, L. Zhou, T. Xu et al., "Antiseptic activity of ethnomedicinal xuebijing revealed by the metabolomics analysis using UHPLC-Q-orbitrap HRMS," *Frontiers in Pharmacology*, vol. 9, p. 300, 2018.

[15] K. Bhumsoo, S. R. Catrina, A. S. Stacey, and L. F. Eva, "Chapter 12 diabetes and cognitive dysfunction," *Neurobiology of Brain Disorders*, Academic Press, pp. 185–201, Cambridge, MA, USA, 2023.

[16] D. A. Bender and P. A. Mayes, "Overview of metabolism: the provision of metabolic fuels," *Harper's Illustrated Biochemistry*, McGraw-Hill Education, pp. 135–136, New York, NY, USA, 2018.

[17] K. C. Patra and N. Hay, "The pentose phosphate pathway and cancer," *Trends in Biochemical Sciences*, vol. 39, no. 8, pp. 347–354, 2014.

[18] K. S. Peters, E. Rivera, C. Warden et al., "Plasma arginine and citrulline are elevated in diabetic retinopathy," *American Journal of Ophthalmology*, vol. 235, pp. 154–162, 2022.

[19] L. W. Chang, L. J. Juang, B. S. Wang et al., "Antioxidant and antityrosinase activity of mulberry (Morus alba L.) twigs and root bark," *Food and Chemical Toxicology*, vol. 49, no. 4, pp. 785–790, 2011.

[20] X. Q. Hu, K. Thakur, G. H. Chen et al., "Metabolic effect of 1-deoxynojirimycin from mulberry leaves on db/db diabetic mice using liquid chromatography mass spectrometry based metabolomics," *Journal of Agricultural and Food Chemistry*, vol. 65, no. 23, pp. 4658–4667, 2017.

[21] Y. Q. Guo, G. H. Tang, L. L. Lou et al., "Prenylated flavonoids as potent phosphodiesterase-4 inhibitors from Morus alba: isolation, modification, and structure-activity relationship study," *European Journal of Medicinal Chemistry*, vol. 144, pp. 758–766, 2018.

[22] X. He, J. Fang, Y. Ruan et al., "Structures, bioactivities and future prospective of polysaccharides from Morus alba (white mulberry): a review," *Food Chemistry*, vol. 245, pp. 899–910, 2018.

[23] J. Cassuto, H. Dou, I. Czikora et al., "Peroxynitrite disrupts endothelial caveolae leading to ENOS uncoupling and diminished flow-mediated dilation in coronary arterioles of diabetic patients," *Diabetes*, vol. 63, no. 4, pp. 1381–1393, 2014.

[24] W. J. Wu, X. X. Liao, Y. Chen, L. N. Ji, and H. Chao, "Mitochondria-targeting and reversible near-infrared emissive iridium (III) probe for in vivo $ONOO^-$/GSH redox cycles monitoring," *Analytical Chemistry*, vol. 93, no. 22, pp. 8062–8070, 2021.

[25] S. M. Adam, G. B. Wijeratne, P. J. Rogler et al., "Synthetic Fe/Cu complexes: toward understanding heme-copper oxidase structure and function," *Chemistry Review*, vol. 118, no. 22, pp. 10840–11022, 2018.

[26] P. Vemula, Y. Jing, H. Zhang et al., "Altered brain arginine metabolism in a mouse model of tauopathy," *Amino Acids*, vol. 51, no. 3, pp. 513–528, 2019.

[27] D. Rogacka, I. Audzeyenka, P. Rachubik et al., "Involvement of nitric oxide synthase/nitric oxide pathway in the regulation of SIRT1–AMPK crosstalk in podocytes: impact on glucose uptake," *Archives of Biochemistry and Biophysics*, vol. 709, Article ID 108985, 2021.

[28] J. Aldred and J. G. Nutt, "Levodopa," *Encyclopedia of Movement Disorders*, vol. 7, pp. 132–137, 2010.

[29] B. Huang, Z. Zhou, J. Liu et al., "The role of monoamine oxidase A in HPV-16 E7-induced epithelial-mesenchymal transition and HIF-1α protein accumulation in non-small cell lung cancer cells," *International Journal of Biological Sciences*, vol. 16, no. 14, pp. 2692–2703, 2020.

[30] A. K. Lee, M. Mojtahed-Jaberi, T. Kyriakou et al., "Effect of high-fat feeding on expression of genes controlling availability of dopamine in mouse hypothalamus," *Nutrition*, vol. 26, no. 4, pp. 411–422, 2010.

[31] Q. An, V. Vaccarino, J. Goldberg, and J. Y. Zhao, "Abstract P366: promoter methylation of the monoamine oxidase a gene is associated with fasting plasma glucose: a monozygotic twin study," *Circulation*, vol. 131, no. suppl_1, pp. 366-367, 2015.

[32] J. Solivan-Rivera, Z. Yang Loureiro, T. DeSouza et al., "A neurogenic signature involving monoamine Oxidase-A controls human thermogenic adipose tissue development," *Elife*, vol. 11, Article ID e78945, 2022.

[33] R. Nagarajrao and S. A. Alharbi, "Relationship between oxidant and antioxidant enzymes status in type 2 diabetic patients with nephropathy in Saudi population," *Asian Journal of Pharmaceutical and Clinical Research*, vol. 11, no. 1, pp. 363-364, 2018.

[34] G. Kuzgun, R. Başaran, E. Arıoğlu İnan, and B. Can Eke, "Effects of insulin treatment on hepatic CYP1A1 and CYP2E1 activities and lipid peroxidation levels in streptozotocin-induced diabetic rats," *Journal of Diabetes and Metabolic Disorders*, vol. 19, no. 2, pp. 1157–1164, 2020.